# Electronic Supplementary Information (ESI)

## Marine Biomass-Derived, Hygroscopic and Temperature-Responsive Hydrogel Beads for Atmospheric Water Harvesting and Solar-Powered Irrigation

Xuemei Chang,[a] Shuai Li,[a] Na Li,[a] Shuxue Wang,[a] Jingjing Li,[a] Cui Guo,[b] Liangmin Yu,[c,d] Petri Murto*,[e] & Xiaofeng Xu*,[a]

[a] College of Materials Science and Engineering, Ocean University of China, Qingdao 266100, China.

[b] College of Marine Life Science, Institute of Evolution & Marine Biodiversity, Ocean University of China, Qingdao 266003, China.

[c] Key Laboratory of Marine Chemistry Theory and Technology, Ministry of Education, Ocean University of China, Qingdao 266100, China.

[d] Open Studio for Marine Corrosion and Protection, Pilot National Laboratory for Marine Science and Technology, Qingdao 266237, China.

[e] Yusuf Hamied Department of Chemistry, University of Cambridge, Cambridge, CB2 1EW, United Kingdom.

* Corresponding authors: X. Xu, email: xuxiaofeng@ouc.edu.cn

P. Murto, email: pm707@cam.ac.uk

# Table of Contents

## 1. Materials

Kelp was harvested on the coast of the Yellow Sea, Qingdao, China. Formaldehyde aqueous solution (37%), concentrated hydrochloric acid (37%), Sodium carbonate anhydrous ($Na_2CO_3$, 99.8%), potassium persulfate ($K_2S_2O_8$, 99.5%) and calcium chloride ($CaCl_2$, 99%) were purchased from Sinopharm Chemical Reagent Co., Ltd. N, N'-Methylenediacrylamide (MBA, 98%) was purchased from Shanghai Macklin Biochemical Co. N-isopropylacrylamide (NIPAM, 98%) was purchased from Zhengzhou Alpha Chemical Co., Ltd. All materials were used directly without further purification.

## 2. Material characterization

Fourier transform infrared (FTIR) spectra were measured via a FTIR spectrometer (iS50 FTIR, Thermo Fisher Scientific). Morphologies and elemental mapping were characterized by a scanning electron microscope (VEGA3, TESCAN) in combination with an energy dispersive X-ray spectrometry. $^1H$ nuclear magnetic resonance (NMR) spectroscopy was measured via NMR spectrometer (Agilent 600M, Agilent). Optical photos of hydrogels were taken through an optical microscope (LEICA MC170 HD). Dynamic mechanical properties of hydrogels are measured via a rheometer (HAAKE, MARS60). Surface wettability was evaluated by an optical contact angle meter (CA, JC2000DM, POWEREACH) equipped with a camera. The phase transition temperature of hydrogel was measured by TOLEDOTM and METTLER. Compressive stress−strain curves of aerogels were measured using a mechanical testing system equipped with a digital force gauge (M5-100, MARK-10) and a force test stand (ESM303, MARK-10). The compression strain rate of aerogels was fixed at 5 mm $min^{-1}$ for the tests. The quality of collected water was tested by inductively coupled plasma mass spectrometry (ICP-MS, Thermo ICAP PRO). Temperature and water content in soil were measured via a soil moisture temperature conductivity sensor (Model 458, VS-3000-TR-PH-N01).

### 3. Preparation of SA from kelp

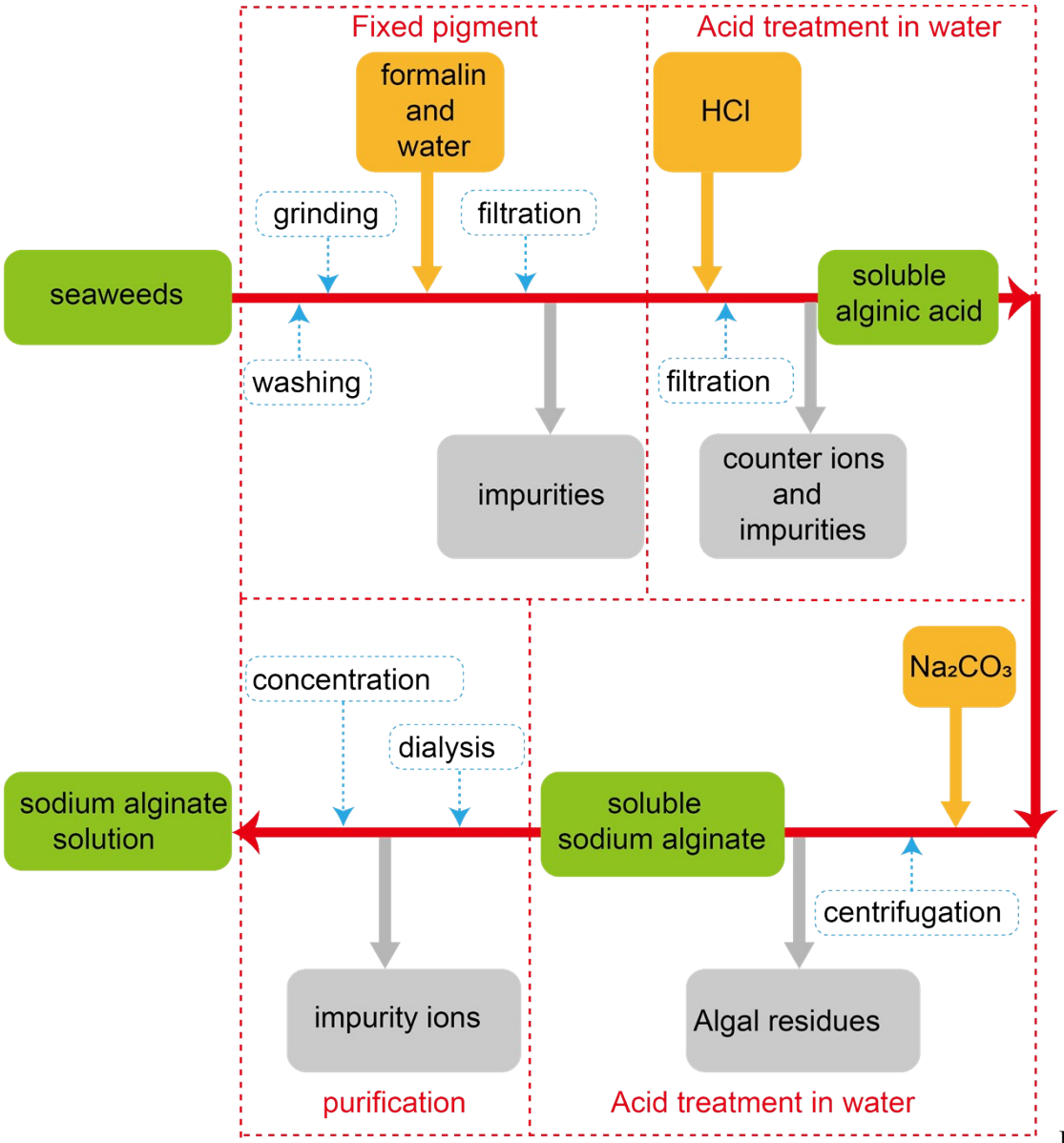


**Figure S1.** A flowchart of extraction and purification of sodium alginate (SA) from kelp.

## 4. Illustration of different chain segments in SA

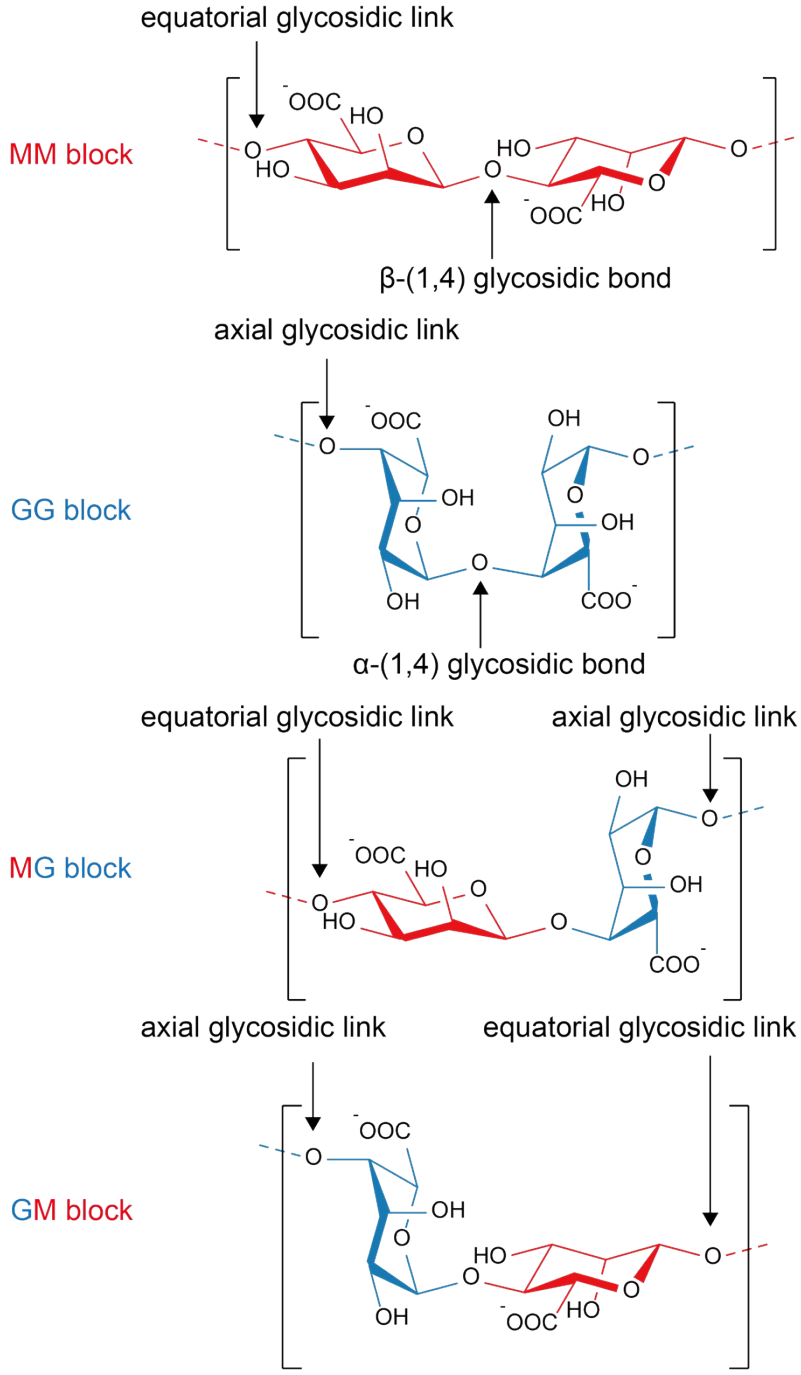


**Figure S2.** Chemical structures of MM, GG, MG and GM building blocks in SA.

## 5. $^1$H NMR characterization

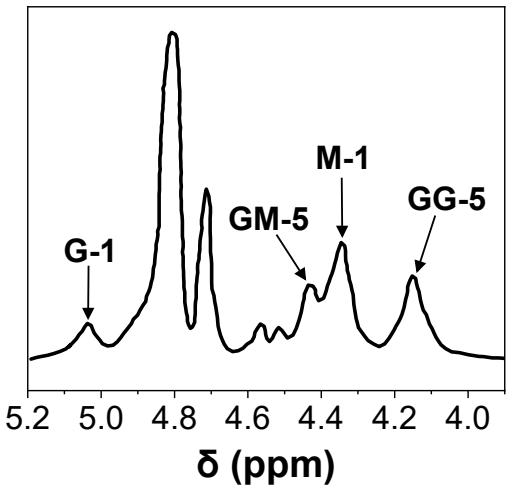


**Figure S3.** $^1$H NMR spectra of extracted SA from kelp.

## 6. FTIR characterization

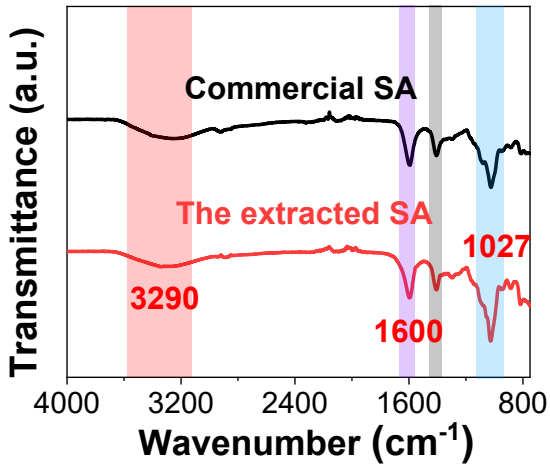


**Figure S4.** FTIR spectra of commercial and as-prepared SA.

## 7. Water vapor sorption characterization

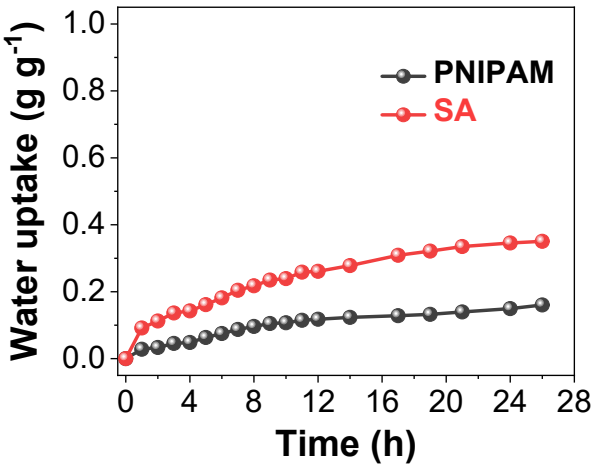


**Figure S5.** Water vapor sorption measurements of neat PNIPAM and SA powder (RH = 90% and temperature = 25 °C).

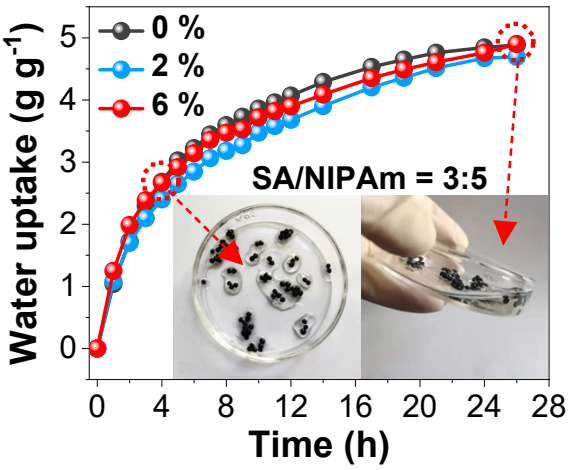


**Figure S6.** Water vapor sorption measurements of *cl*-SP beads with different ink concentration (0%, 2% and 6%, w/w) (RH = 90% and temperature = 25 °C).

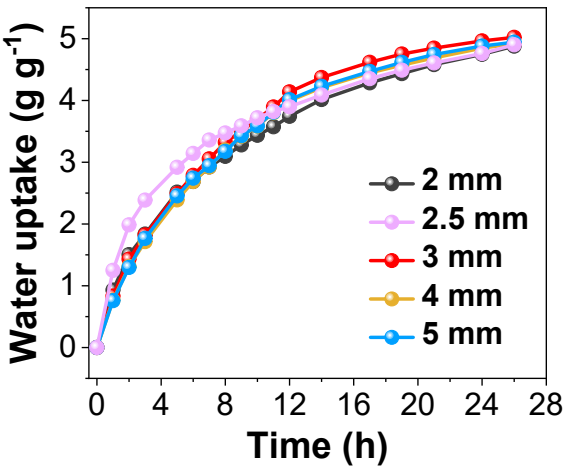


**Figure S7.** Water vapor sorption measurements of *cl*-SP beads with different diameters (2, 2.5, 3, 4 and 5 mm) (RH = 90% and temperature of = 25 °C).

## 8. Water vapor sorption rates

**Table S1.** Water vapor sorption rates of *cl*-SP and ALG-Ca beads (RH = 90% and temperature = 25 °C).

| Sample | RH (%) | $R_s$ ($h^{-1}$) |
|---|---|---|
| *cl* -SP (1:5) | 90 | 0.146 |
| *cl* -SP (2:5) | 90 | 0.164 |
| *cl* -SP (3:5) | 90 | 0.208 |
| *cl* -SP (4:5) | 90 | 0.195 |
| *cl* -SP (5:5) | 90 | 0.186 |
| ALG-Ca | 90 | 0.184 |

## 9. Water vapor sorption kinetics

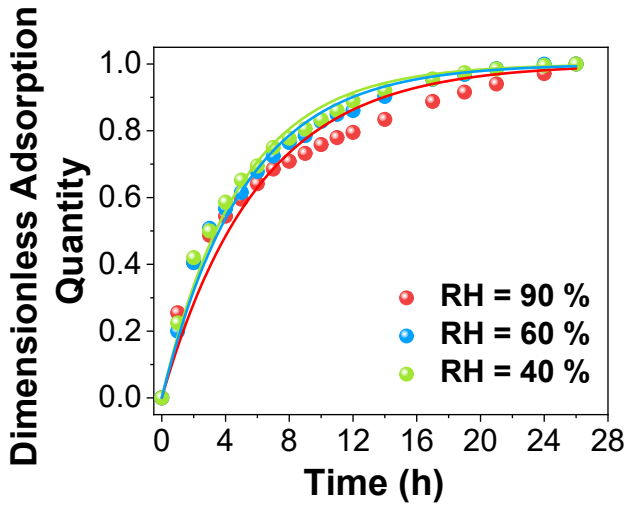


**Figure S8.** Kinetic curves of *cl*-SP beads (3:5) under 40%, 60% and 90% RH.

**Table S2.** Kinetic parameters of water vapor sorption under different RH.

| Samples | RH (%) | Kinetic equations | $k$ ($h^{-1}$) | $R^2$ |
|---|---|---|---|---|
| *cl*-SP (3:5) | 90 | $y = 1 - e^{-0.16569\ t}$ | 0.16569 | 0.9475 |
| *cl*-SP (3:5) | 60 | $y = 1 - e^{-0.1928\ t}$ | 0.1928 | 0.98563 |
| *cl*-SP (3:5) | 30 | $y = 1 - e^{-0.20481\ t}$ | 0.20481 | 0.98734 |

## 10. Specific surface area characterization

**Table S3.** Specific surface area of different samples.

| Shapes | Surface area ($cm^2$) | Specific surface area ($cm^2\ g^{-1}$) |
|---|---|---|
| bead | 4.15 | 8.30 |
| rectangle | 2.50 | 5.00 |
| triangle | 2.42 | 4.84 |
| cylinder | 2.33 | 4.66 |

## 11. Water vapor sorption under low RH

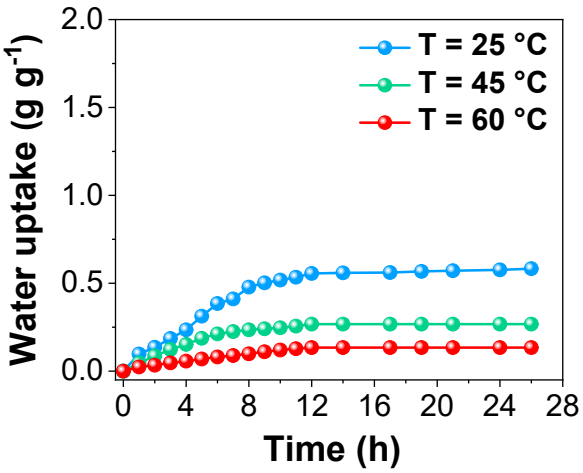


**Figure S9.** Water vapor sorption measurements of *cl*-SP beads with different temperatures (RH = 25%).

## 12. Equilibrium of water vapor sorption

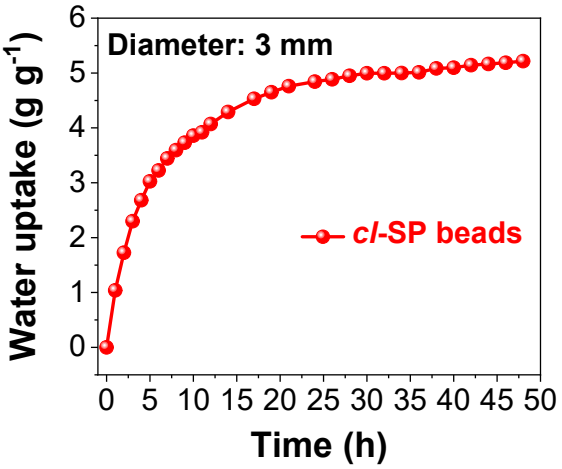


**Figure S10.** Water vapor sorption of *cl*-SP beads under RH = 90% and temperature = 25 °C.

## 13. XPS spectra

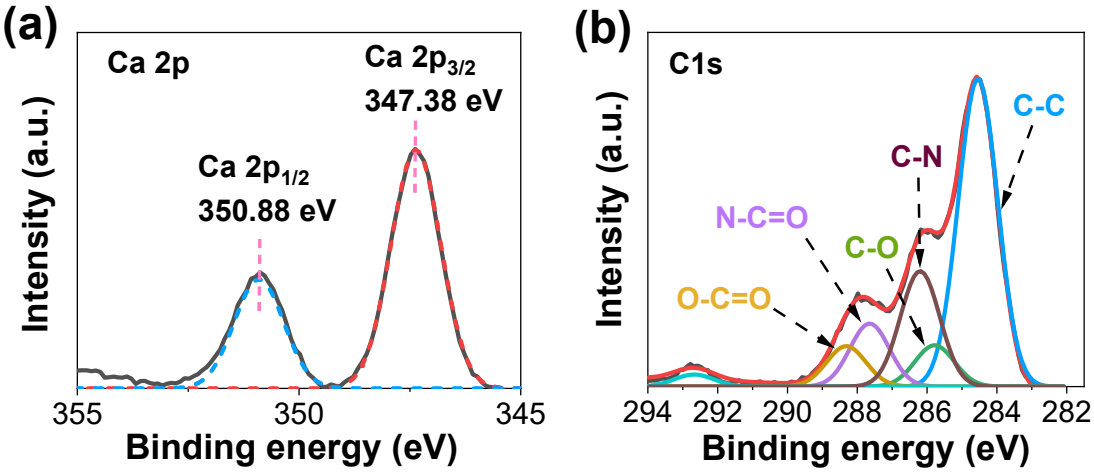


**Figure S11.** High resolution XPS spectra of (a) Ca 2p and (b) C1s of *cl*-SP beads.

## 14. Dynamic rheological properties

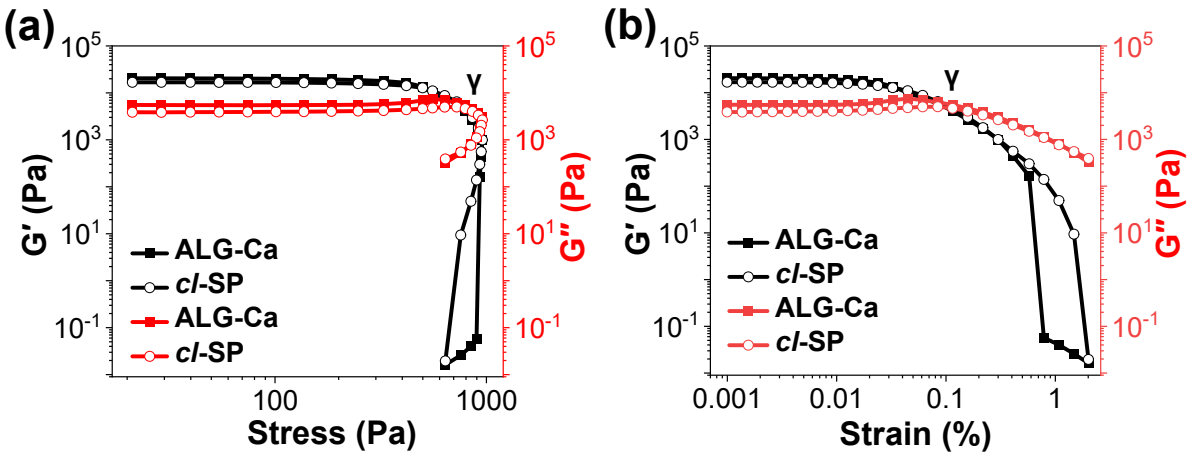


**Figure S12.** G' and G'' of *cl*-SP gels under (a) stress and (b) strain sweep.

## 15. Cyclic compression experiments

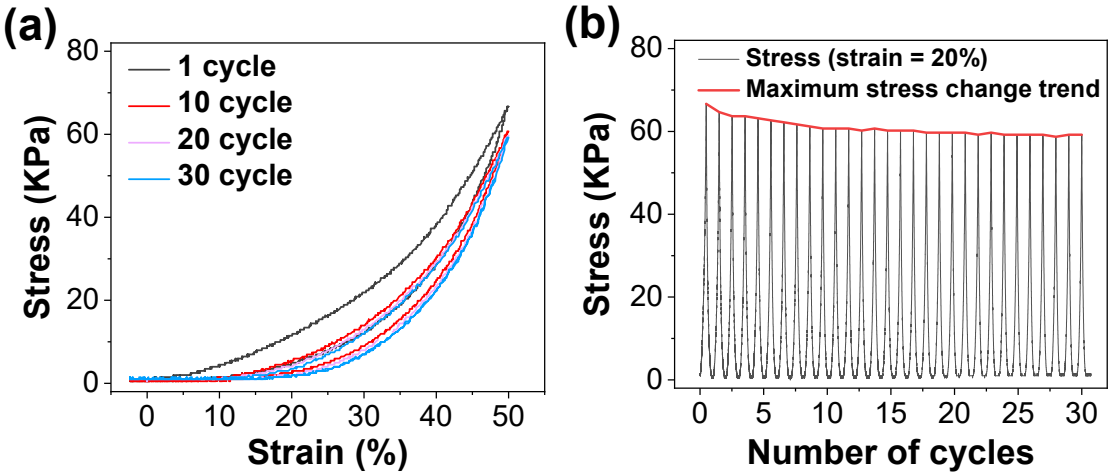


**Figure S13.** (a) Compressive stress−strain curves and (b) stress variations over loading/releasing cycles of *cl*-SP hydrogels.

## 16. Absorption spectra of *cl*-SP composites

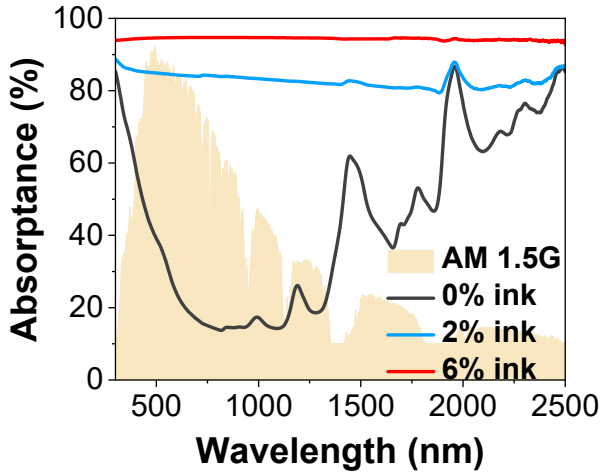


**Figure S14.** Absorbance spectra of *cl*-SP beads with different ink concentrations and the solar spectrum.

## 17. EDS mapping of *cl*-SP beads

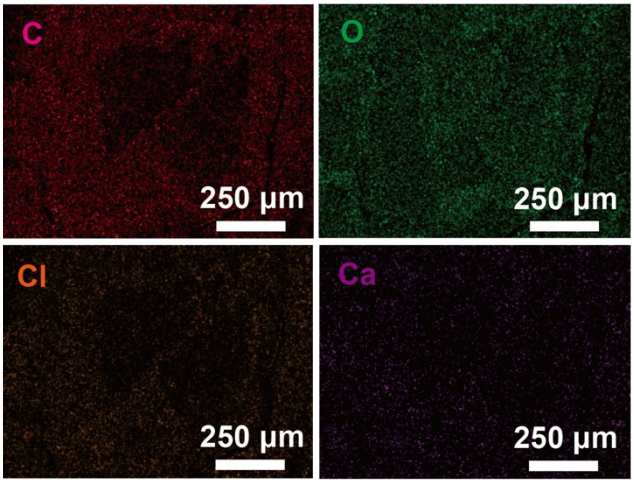


**Figure S15.** EDS images of *cl*-SP beads.

## 18. Calculation of photothermal conversion efficiencies

The solar-to-vapor efficiency was calculated using Equation S1,

$$\eta = \frac{\Delta m \times h_{lv}}{P_{in}} \qquad \text{(S1)}$$

where Δm is the net evaporation rate, $h_{lv}$ is the total enthalpy of sensible heat and phase change of liquid to water (2450 J $g^{-1}$), $P_{in}$ is the power of the incident simulated sunlight beam (1 kW $m^{-2}$). In our experimental, $\Delta m$ = 1.05 kg $m^{-2}$ $h^{-1}$. The average photothermal conversion efficiency of the *cl*-SP (3:5) beads was calculated to be 71.5%.

## 19. Water desorption rate under different solar intensity

**Table S4.** Water desorption rates of *cl*-SP (3:5) beads under different solar intensity.

| Samples | Solar intensity (kW $m^{-2}$) | $R_d$ ($h^{-1}$) |
|---|---|---|
| *cl*-SP (3:5) | 1.0 | 0.213 |
| *cl*-SP (3:5) | 0.9 | 0.201 |
| *cl*-SP (3:5) | 0.8 | 0.199 |
| *cl*-SP (3:5) | 0.7 | 0.197 |
| *cl*-SP (3:5) | 0.6 | 0.196 |
| ALG-Ca | 1.0 | 0.198 |
| ALG-Ca | 0.6 | 0.137 |

## 20. Water desorption characterization of ALG-Ca beads

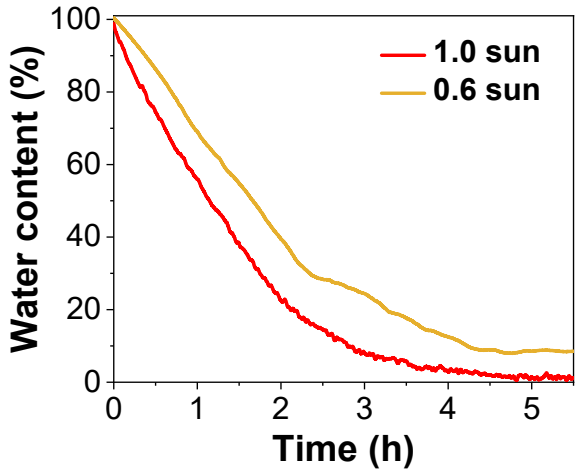


**Figure S16.** Water desorption of neat ALG-Ca beads under 0.6 and 1 sun.

## 21. Water desorption rate under different temperature

**Table S5.** Water desorption rates of *cl*-SP (3:5) beads under different temperature.

| Samples | Desorption temperature (°C) | $R_d$ ($h^{-1}$) |
|---|---|---|
| *cl*-SP (3:5) | 23 | 0.236 |
| *cl*-SP (3:5) | 25 | 0.244 |
| *cl*-SP (3:5) | 30 | 0.257 |
| *cl*-SP (3:5) | 40 | 0.294 |
| *cl*-SP (3:5) | 50 | 0.310 |
| *cl*-SP (3:5) | 60 | 0.313 |

## 22. Arrhenius plots

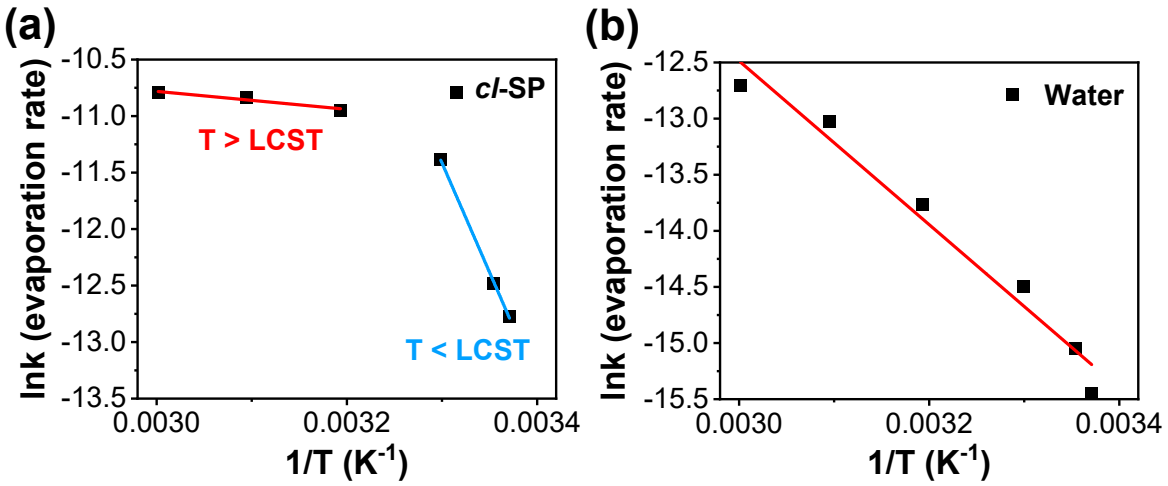


**Figure S17.** Arrhenius plots of (a) *cl*-SP beads and (b) neat water.

Activation energy of water evaporation is calculated using the Arrhenius equation:

$$k = A \times e^{\frac{-Ea}{RT}} \qquad \text{(S2)}$$

where $k$ is the evaporation rate per unit area (mol $s^{-1}$ $cm^{-2}$), $A$ is the pre-exponential factor, $E_a$ is the activation energy (kJ $mol^{-1}$), $R$ is the universal gas constant (8.314 × $10^{-3}$ kJ $K^{-1}$ $mol^{-1}$) and $T$ is the absolute temperature (K).

## 23. Clean water production characterization

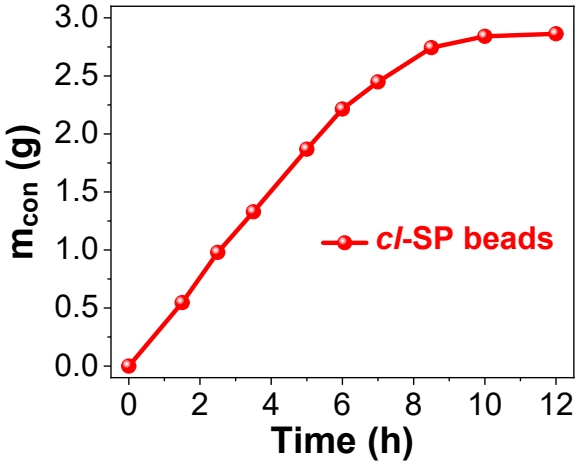


**Figure S18.** Mass changes of condensed water over time under 1 sun.

## 24. SEM images of *cl*-SP beads over sorption/adsorption cycles

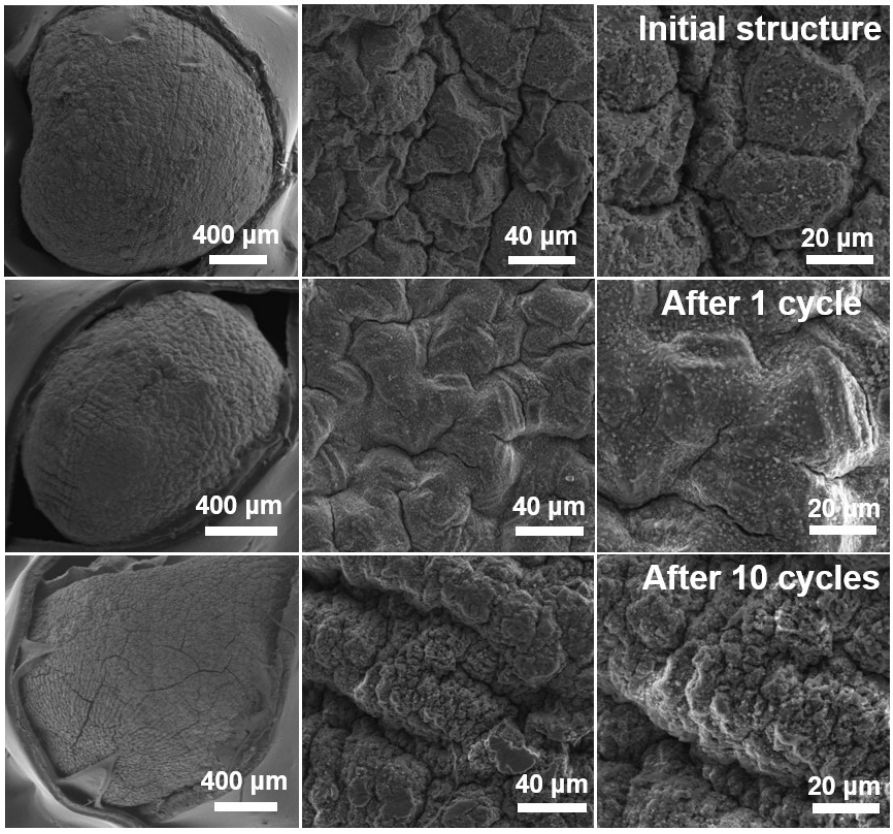


**Figure S19.** SEM images of *cl*-SP beads in different sorption/adsorption cycles.

## 25. EDS mapping after sorption/adsorption cycles

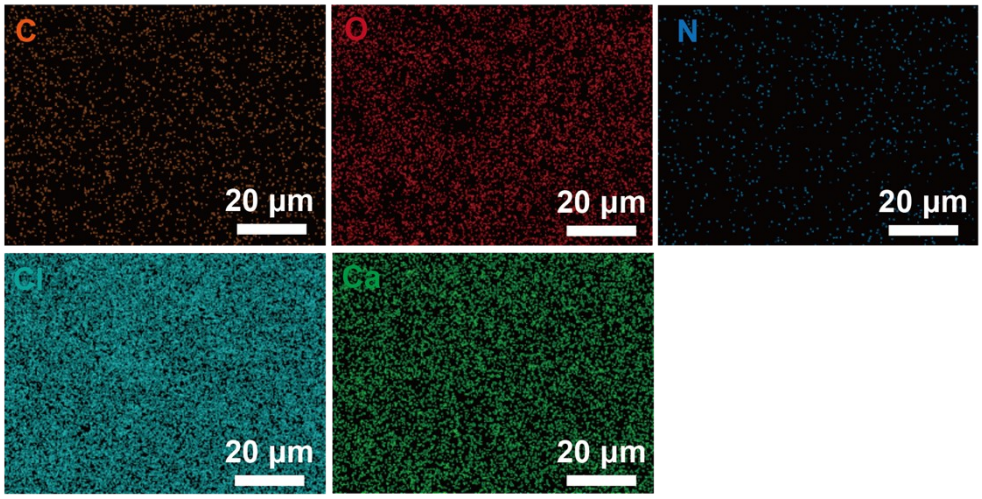


**Figure S20.** EDS images of *cl*-SP beads after 10 cycles of sorption/adsorption.

## 26. Summary of AWG performance

**Table S6.** Summary of AWG performance reported in recent years.

| AWGs | RH (%) | Water uptake (g $g^{-1}$) | Plant cultivation |
|---|---|---|---|
| PAM-LiCl[1] | 10<br>20<br>30 | 0.5<br>1.1<br>1.5 | No |
| HSCC-E10[2] | 90<br>70<br>30 | 3.75<br>2.83<br>1.47 | No |
| CMCS-Ca@SF[3] | 90 | 1.35 | No |
| PFVD[4] | 98 | 4.34 | No |
| HMC-2[5] | 90<br>60<br>40 | 1.074<br>1.919<br>0.345 | No |
| PDMAPS-LiCl[6] | 30 | 0.62 | No |
| SHPFs[7] | 30<br>15 | 0.96<br>0.64 | No |
| CACS[8] | 80<br>40<br>35 | 0.45<br>0.40<br>0.29 | No |
| CAS[9] | 35 | 0.31 | No |
| IMFCA[10] | 80<br>20 | 2.30<br>0.50 | No |
| LBC@LiCl[11] | 90 | 2.47 | No |

| | | | |
|---|---|---|---|
| | 60 | 1.12 | |
| | 40 | 0.81 | |
| PAETA-Ac[12] | 80 | 0.87 | No |
| | 30 | 0.31 | |
| | 80 | 2.73 | |
| GO-SSNFs[13] | 60 | 1.76 | No |
| | 30 | 0.96 | |
| NBHA[14] | 95 | 2.36 | No |
| | 35 | 0.30 | |
| | 90 | 1.5 | |
| ILCA[15] | 60 | 1.2 | No |
| | 30 | 0.5 | |
| | 90 | 4.2 | |
| PC-MOF[16] | 60 | 1.6 | No |
| | 30 | 0.8 | |
| Bina/FCNT[17] | 70 | 5.60 | No |
| | 20 | 1.40 | |
| | 100 | 1.88 | |
| HEPF[18] | 60 | 1.15 | No |
| | 40 | 1.04 | |
| | 90 | 6.70 | |
| SMAGs[19] | 60 | 3.40 | No |
| | 30 | 0.70 | |
| Zn hydrogel[20] | 90 | 2.3 | No |
| $MgCl_2$ particles incorporated into an alginate-derived[21] | 30 | 0.93 | No |
| Alg-$CaCl_2$(78 wt%)[22] | 26 | 1.0 | No |
| ACF-Silica Sol-LiCl[23] | 70 | 1.4 | No |
| | 20 | 0.5 | |
| | 80 | 1.73 | |
| PAM-CNT-$CaCl_2$[24] | 60 | 1.10 | No |
| | 35 | 0.69 | |
| $CaCl_2$@UiO[25] | 70 | 1.0 | No |

## 27. Water quality characterization

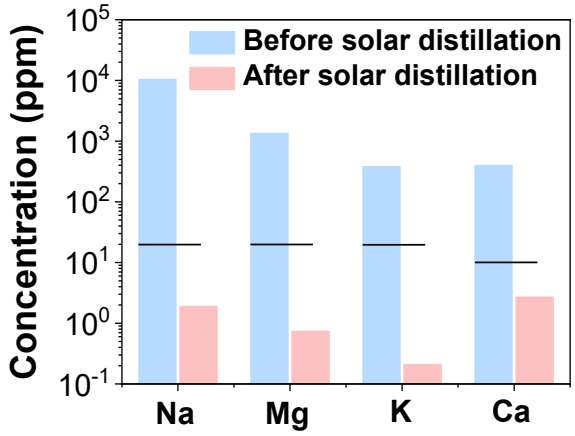


**Figure S21.** Primary element concentration before and after solar distillation. (Black lines show WHO quality standards required for safe drinking water).

## 28. Summary of reference crop evapotranspiration

**Table S7.** Average daily water requirement of standard grass during irrigation seasons.

| Climatic zones | Mean daily temperature | | |
|---|---|---|---|
| | low (less than 15 °C) | medium (15−25 °C) | high (more than 25 °C) |
| Desert/arid | 4−6 | 7−8 | 9−10 |
| Semi-arid | 4−5 | 6−7 | 8−9 |
| Sub-humid | 3−4 | 5−6 | 7−8 |
| Humid | 1−2 | 3−4 | 5−6 |

## 29. Solar intensity, RH and soil temperature

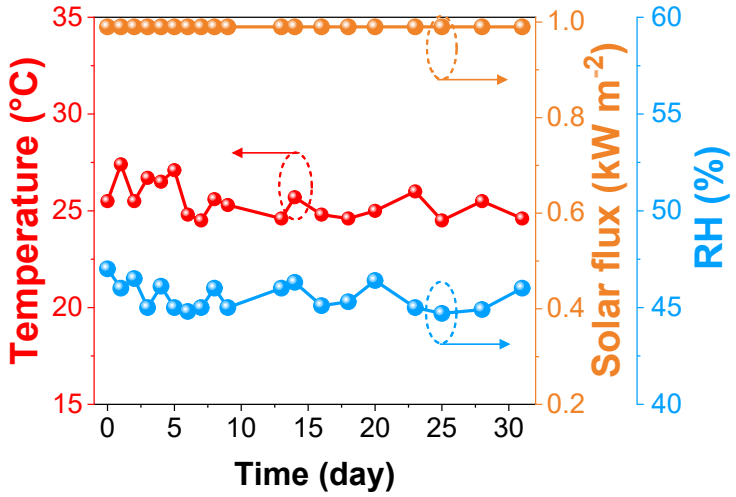


**Figure S22.** Changes of solar intensity, RH and soil temperature over 30 days.

## 30. Digital photographs of clover growth

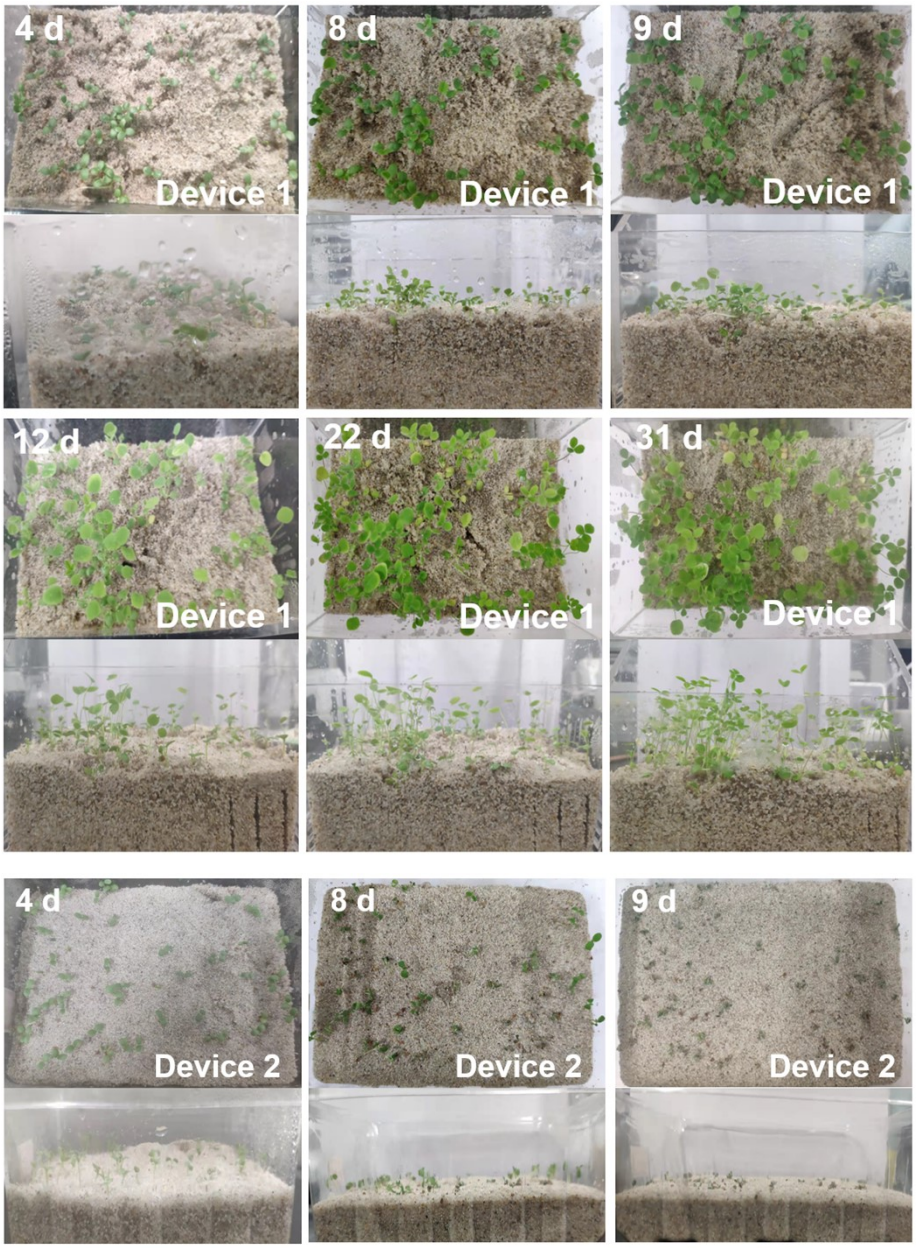


**Figure S23.** Digital photographs of clover growth in Devices 1 and 2 over 30 days.

## 31. Root and bud length of clover

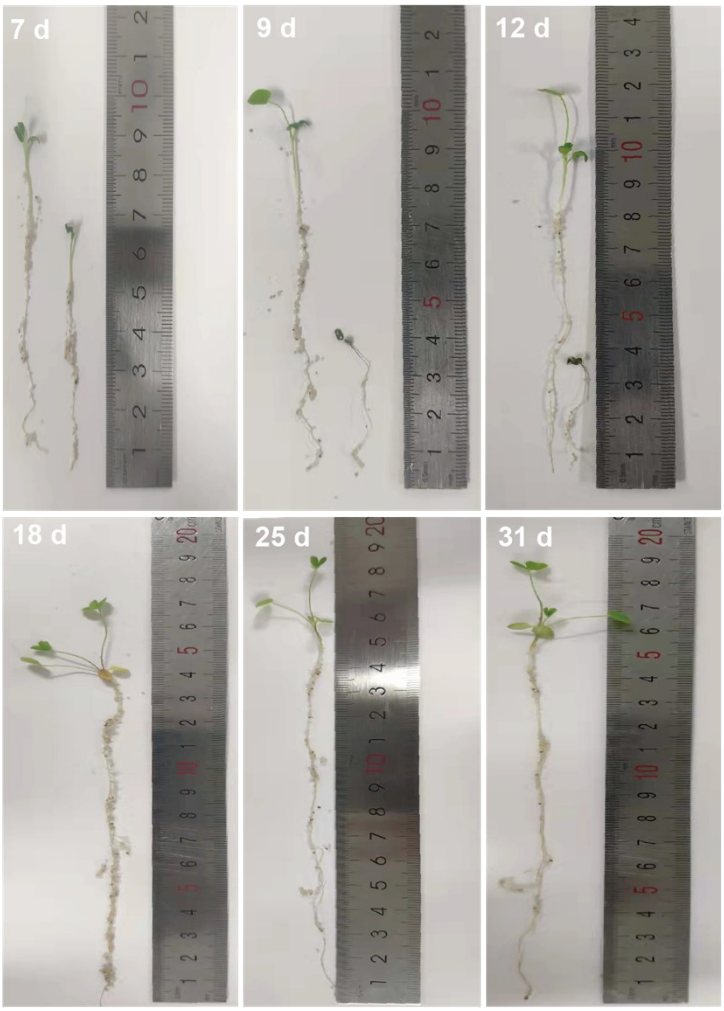


**Figure S24.** Digital photographs of root and bud length of clover in Device 1 over 30 days.

## 32. Degradation of *cl*-SP beads

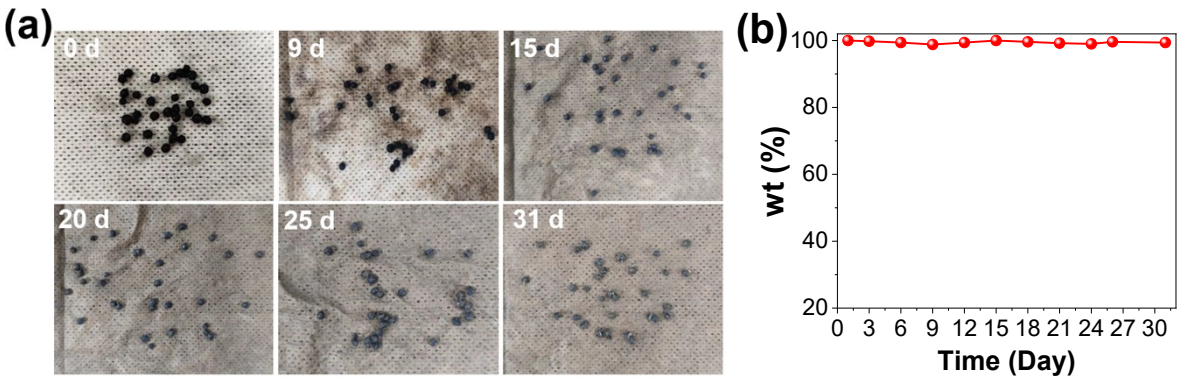


**Figure S25.** (a) Digital photographs and (b) mass changes of *cl*-SP beads in the soil over 30 days.

## 33. Reference


[1] H. Lu, W. Shi, J. H. Zhang, A. C. Chen, W. Guan, C. Lei, J. R. Greer, S. V. Boriskina, G. Yu, *Adv. Mater.* **2022**, DOI: 10.1002/adma.202205344.
[2] H. Shan, Q. Pan, C. Li, R. Wang, *STAR Protoc* **2022**, 3, 101255.
[3] Y. Nong, B. Fan, X. Bao, B. Xu, M. Zhou, Y. Yu, Q. Wang, P. Wang, *Mater Today Commun.* **2022**, 32, 103984.
[4] T. Lyu, Z. Wang, R. Liu, K. Chen, H. Liu, Y. Tian, *ACS Appl. Mater. Inter.* **2022**, 14, 32433.
[5] Y. Hu, Z. Fang, X. Wan, X. Ma, S. Wang, S. Fan, M. Dong, Z. Ye, X. Peng, *Chem. Eng. J.* **2022**, 430, 133086.
[6] C. Lei, Y. Guo, W. Guan, H. Lu, W. Shi, G. Yu, *Angew. Chem. Int. Edit.* **2022**, 61, e202200271.
[7] Y. Guo, W. Guan, C. Lei, H. Lu, W. Shi, G. Yu, *Nat. Commun.* **2022**, 13, 2761.
[8] Y. Tao, Q. Wu, C. Huang, W. Su, Y. Ying, D. Zhu, H. Li, *ACS Appl. Mater. Inter.* **2022**, 14, 10966.
[9] Q. Li, Y. Ying, Y. Tao, H. Li, *Ind. Eng. Chem. Res.* **2022**, 61, 1344.
[10] F. F. Deng, C. J. Xiang, C. X. Wang, R. Z. Wang, *J. Mater. Chem. A.* **2022**, 10, 6576.
[11] W. Yao, X. Zhu, Z. Xu, R. A. Davis, G. Liu, H. Zhong, X. Lin, P. Dong, M. Ye, J. Shen, *ACS Appl. Mater. Inter.* **2022**, 14, 4680.
[12] M. Wu, R. Li, Y. Shi, M. Altunkaya, S. Aleid, C. Zhang, W. Wang, P. Wang, *Mater. Horiz.* **2021**, 8, 1518.
[13] S. Kim, Y. Liang, S. Kang, H. Choi, *Chem. Eng. J.* **2021**, 425, 131601.
[14] M. Z. Wang, T. M. Sun, D. H. Wan, M. Dai, S. J. Ling, J. L. Wang, Y. Q. Liu, Y. Fang, S. H. Xu, J. J. Yeo, H. P. Yu, S. X. Liu, Q. W. Wang, J. Li, Y. Yang, Z. J. Fan, W. S. Chen, *Nano Energy* **2021**, 80, 105569.
[15] F. F. Deng, C. X. Wang, C. J. Xiang, R. Z. Wang, *Nano Energy* **2021**, 90, 106642.
[16] G. Yilmaz, F. L. Meng, W. Lu, J. Abed, C. K. N. Peh, M. Gao, E. H. Sargent, G. W. Ho, *Sci. Adv.* **2020**, 6, eabc8605.
[17] A. Entezari, M. Ejeian, R. Z. Wang, *ACS Mater. Lett.* **2020**, 2, 471.
[18] S. L. Loo, L. Vasquez, U. C. Paul, L. Campagnolo, A. Athanassiou, D. Fragouli, *ACS Appl. Mater. Inter.* **2020**, 12, 10307.

[19] F. Zhao, X. Zhou, Y. Liu, Y. Shi, Y. Dai, G. Yu, *Adv. Mater.* **2019**, 31, 1806446.
[20] D. K. Nandakumar, S. K. Ravi, Y. X. Zhang, N. Guo, C. Zhang, S. C. Tan, *Energ. Environ. Sci.* **2018**, 11, 2179.
[21] P. A. Kallenberger, K. Posern, K. Linnow, F. J. Brieler, M. Steiger, M. Froba, *Adv. Sustain. Syst.* **2018**, 2, 1700160.
[22] P. A. Kallenberger, M. Fröba, *Commun. Chem.* **2018**, 1, 28.
[23] J. Y. Wang, R. Z. Wang, Y. D. Tu, L. W. Wang, *Energy* **2018**, 165, 387.
[24] R. Li, Y. Shi, M. Alsaedi, M. Wu, L. Shi, P. Wang, *Environ. Sci. Technol.* **2018**, 52, 11367.
[25] L. Garzón-Tovar, J. Pérez-Carvajal, I. Imaz, D. Maspoch, *Adv. Funct. Mater.* **2017**, 27, 1606424.